Microstructure of $SiO_2-Al_2O_3-CaO-P_2O_5-K_2O-F^-$ Glass Ceramics. 2. Time Dependence of Apatite Crystal Growth

Thomas Höche,*,† Cornelia Moisescu, Issak Avramov,‡ and Christian Rüssel

Otto-Schott-Institut für Glaschemie, Friedrich-Schiller-Universität, Fraunhoferstrasse 6, D-07743 Jena, Germany

Wolfgang D. Heerdegen and Christian Jäger

Institut für Optik und Quantenelektronik, Friedrich-Schiller-Universität Jena, Max-Wien-Platz 1, D-07743 Jena, Germany

Received October 17, 2000. Revised Manuscript Received January 8, 2001

It is shown that fluorapatite needles formed in $SiO_2-Al_2O_3-CaO-P_2O_5-K_2O-F^-$ glasses upon heat treatment at 1200 °C undergo a time-dependent coarsening that fulfills the criteria of Ostwald ripening. Thermodynamic considerations imply that different growth mechanisms (normal and spiral growth) along different crystallographic directions are responsible for the strongly direction-dependent growth rates observed at 1200 °C, leading to an apatite-needle aspect ratio as large as 15:1 after 15 h at 1200 °C. The microstructure is textured by postcrystallization extrusion, facilitating a thorough investigation of the apatite needle morphology and the determination of anisotropic crystal-growth rates. During very long-term heat treatments at 1200 °C, however, the formation of isometric, blocklike apatite crystals is encountered. The latter crystals are formed at the expense of apatite needles and their occurrence proves that the needle morphology is not a result of the equilibrium shape but caused by kinetic growth effects. But although the transition from the growth habit to the equilibrium shape limits the maximum aspect ratio of fluorapatite needles (15:1), the extruded glass ceramics exhibit an extraordinary degree of texturing.

1. Introduction

In the companion article,[1] the rationale for the development of fluorapatite containing glass ceramics (GCs) are detailed and it is shown that within the same glass system—depending on the thermal treatment—fluorapatite crystals can either grow isometrically or become needlelike-shaped.

Apatite needles can be readily oriented by the application of postcrystallization extrusion. Since grain orientation within extruded GCs is most effective if crystals with well-expressed anisotropic morphologies are present, the investigation of the time-dependent needle shape of FAp crystals is of high practical relevance.

Therefore, the time dependence of apatite-needle growth is studied by combining ^{31}P MAS NMR, electron microscopic imaging, and energy-dispersive X-ray spectrometry in the transmission electron microscope. The excellent texturing of grain-oriented apatite GCs caused by postcrystallization extrusion[2] also highly facilitates their microstructural characterization.

Table 1. Length, Diameter, Aspect Ratio, and Volume of Apatite Needles vs Annealing Time at 1200 °C[a]

duration of heat treatment at 1200 °C (min)	apatite-needle length (μm)	apatite-needle width (μm)	aspect ratio	apatite-crystal volume (μm^3)
0	$(0.5 \pm 0.03)^b$	$(0.5 \pm 0.03)^b$	1:1	0.07 ± 0.012
2	0.93 ± 0.03	0.44 ± 0.07	2.1:1	0.12 ± 0.004
5	1.80 ± 0.08	0.78 ± 0.03	2.3:1	0.71 ± 0.03
30	2.34 ± 0.09	0.81 ± 0.02	2.9:1	1.0 ± 0.04
120	5.30 ± 0.25	0.97 ± 0.26	5.5:1	3.24 ± 0.15
600	11.42 ± 0.5	1.48 ± 0.38	7.7:1	16.25 ± 1.50
900	23.0 ± 1.2	1.54 ± 0.41	14.9:1	35.4 ± 3.78

[a] Error bars given are standard errors. As can be seen from Figure 5, the standard deviation is much larger in most cases. Volumes and errors of apatite needles were calculated according to the formulas $V = 3/8(3^{1/2}) \cdot W^2 \cdot Z$ and $\delta V = 3/8(3^{1/2})[((\Delta W)^2/2) \cdot W \cdot Z + \Delta Z \cdot W^2]$. [b] Needle-shaped apatite not yet present (width = length = diameter).

2. Experimental Section

In part 1 of this two-part contribution,[1] the synthesis of the base glass is detailed (see Table 1 therein for the chemical composition).

Thermal treatment at 800 or 1200 °C (after insertion of the samples into a preheated furnace, heating rate: $\approx 20\ K \cdot s^{-1}$) converted the cast glass into GCs. Afterward, the already heat-treated samples were extruded using a materials testing apparatus (Zwick 1445) as reported by Roeder.[3] The extrusion was performed with a constant extrusion rate of $2\ mm \cdot min^{-1}$ at 700 °C in the viscosity range of 10^6-10^8 dPa·s using an electrographite die with a circular bore (5 mm diameter). Thermal equilibrium within the cylindrical samples (21.5 mm

* To whom correspondence should be addressed. Fax: +49 3641 948 502. E-mail: hoeche@glas.chemie.uni-jena.de.

† Current address: Lehrstuhl für Kristallographie, Institut für Physik, Humboldt-Universität zu Berlin, Invalidenstrasse 110, D-10115 Berlin, Germany.

‡ On leave from the Institute for Physical Chemistry, Bulgarian Academy of Sciences, 1113 Sofia, Bulgaria.: avramov@ipchp.ipc.bas.bg.

(1) Höche, T.; Moisescu, C.; Avramov, I.; Rüssel, C.; Heerdegen, W. D. *Chem. Mater.* **2001**, *13*, 1312.

(2) Moisescu, C.; Jana, C.; Habelitz, S.; Carl, G.; Rüssel, C. *J. Non-Cryst. Solids* **1999**, *248*, 176.

(3) Roeder, E. *J. Non-Cryst. Solids* **1970/71**, *5*, 377.

10.1021/cm001204h CCC: $20.00
Published on Web 03/14/2001

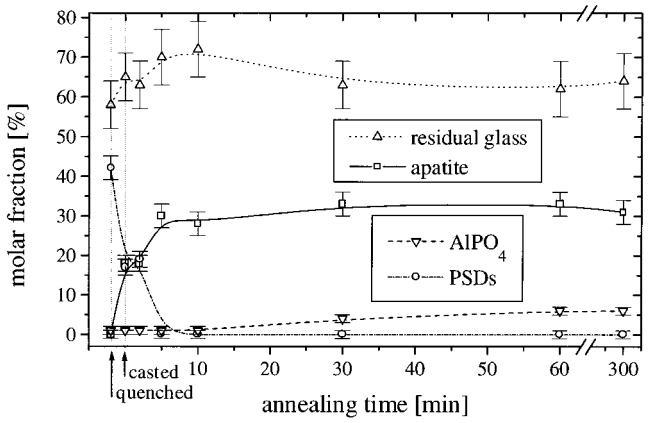

Figure 1. Annealing time dependence of microstructural constituents molar fractions (from ^{31}P MAS NMR data, corrected for compositional variations). Note that separate values are given for the quenched and the cast sample without annealing. Error bars represent standard errors.

diameter, 20 mm height) was established by soaking the samples for about 20 min prior to the extrusion process.

Also, the experimental techniques applied to characterize the microstructure (transmission electron microscopy of replica films as well as transmission samples and ^{31}P MAS NMR) are identical to those described in the companion article.[1] For TEM-EDXS analyses, an average over about 10 independent measurements was calculated for each data point. Because of the very long repetitions times used in the ^{31}P MAS NMR experiments (600 s), only one sample of some 160 mg was measured for each annealing step.

3. Results and Discussion

3.1. Time Dependence of Fluorapatite Crystal Growth at 800 °C. In Figure 1, the evolution of composition-corrected molar fractions, x (introduced in part 1 of this contribution) of the glass matrix (GM), phase separation droplets (PSDs), fluorapatite crystals (FAp), and $AlPO_4$ crystals upon thermal treatment at 800 °C is depicted. In the cast glass, the majority of the PSDs (which are completely "frozen in" in the quenched sample) is converted into FAp and only a minor fraction is dissolved in the ambient glass. A 2-min long heat treatment has almost no effect on the FAp:PSD:GM ratio but already after 5 min, all PSDs have disappeared. As compared to the cast glass, about two-thirds of the PSDs is converted into crystalline FAp (its molar fraction rises to 30%) and one-third of the PSDs is dissolved in the GM. After 30 min, a redistribution of aluminum and phosphorus in the GM has led to the crystallization of $AlPO_4$, the molar fraction of which reaches its maximum of 6% after 60 min and remains constant for longer annealing times. The data indicate that the occurrence of $AlPO_4$ may cause a slight dissolution of FAp in the GM prior to the adjustment of the phase equilibrium after 5 h at 800 °C.

At first glance, the time dependence of the apatite-crystal diameter (Figure 2) seems to be erroneous because after 5 min at 800 °C the crystal size becomes reduced by one-third after a moderate increase from 500 to 550 nm within the first 2 min of heat treatment. Already after 10 min, a much larger average diameter of some 750 nm is found remaining approximately unchanged after 300 min of thermal treatment. The sharp cusp in the diameter versus annealing time plot,

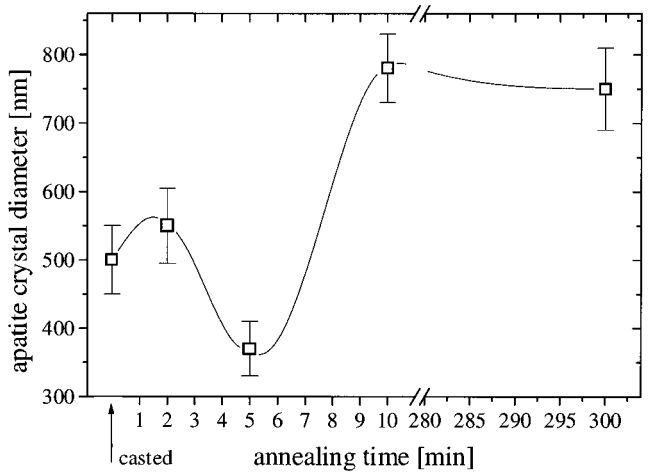

Figure 2. Diameter of isometric apatite crystals observed at 800 °C vs duration of the heat treatment. Individual data points represent averages over at least 50 crystals and error bars correspond to standard deviations. The connecting line is intended to serve as a guide to the eye.

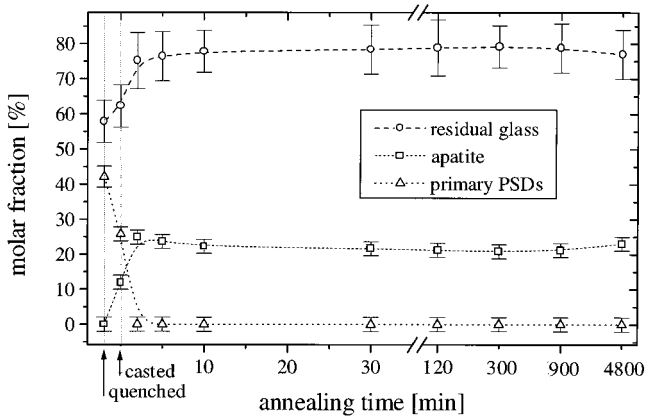

Figure 3. Molar fraction of microstructural constituents vs annealing time (^{31}P MAS NMR data corrected for compositional variations). Again, separate values are given for the quenched and the cast sample. Error bars represent standard errors.

however, can be explained considering the fact that, after 5 min, PSDs have disappeared (the supersaturation is highest) and between 2 and 5 min of tempering a considerable fraction of PSDs is converted into apatite crystals. If the large PSDs crystallize first (between 0 and 2 min) and smaller ones are following later (between 2 and 5 min), the average size will be decreased after 5 min. Upon longer annealing, some coarsening of the particle size occurs but this was not studied in detail because this work focuses on the investigation of needlelike fluorapatite.

3.2. Time Dependence of Fluorapatite Crystal Growth at 1200 °C. While the maximum molar fraction of FAp obtained at 800 °C is 33% (cf. Figure 1), the thermal treatment at 1200 °C results in a maximal molar fraction of 25% only (Figure 3). This value is adjusted within 2 min since diffusion processes are much more rapid at 1200 °C and PSDs are no longer present after 2 min. With longer ceramming times, the molar fraction of apatite remains constant. Contrary to the heat treatment at 800 °C, the formation of $AlPO_4$ does not occur at 1200 °C.

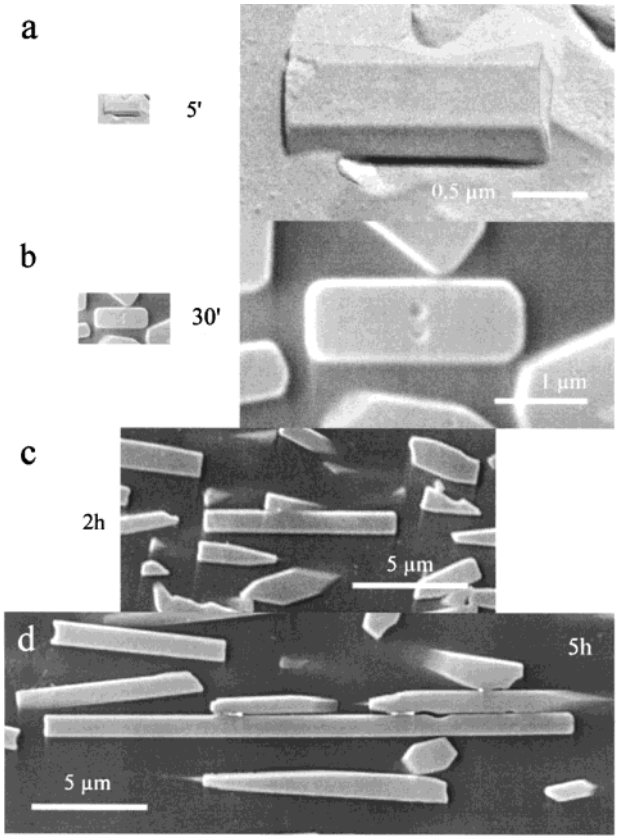

Figure 4. Typical electron micrographs of samples heat-treated for 5 min (TEM replica film) 30 min, 2 h, and 5 h (SEM, secondary-electron image). The left column of images a and b has the same magnification as the two micrographs on the bottom.

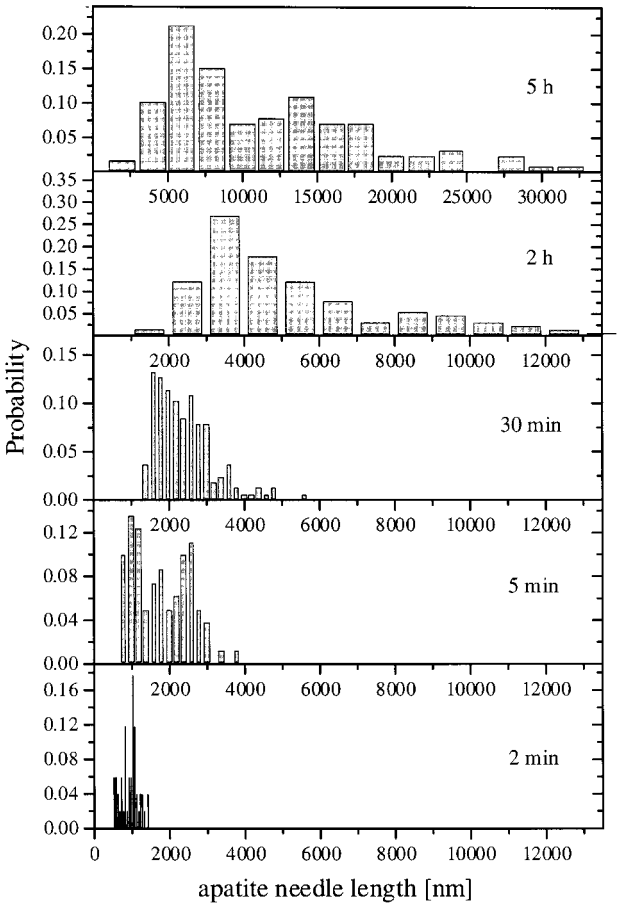

Figure 5. FAp needle-length distribution [determined by careful analyses of TEM replica films and SEM micrographs (cf. Figure 4) as detailed in the text] upon heat treatment at 1200 °C.

In Figure 4, selected examples of apatite needles after heat treatments at 1200 °C for different annealing times are depicted. The uppermost image (5 min) is a TEM replica micrograph and the other images (30 min, 2 and 5 h) were taken in the SEM. The juxtaposition of for example Figures 4a and 4d shows that TEM replica films do reflect a great deal more topographic information in comparison to SEM micrographs. Thus, the measurement of needle lengths and diameters that shall be described in the following are more accurate when replica films are used. But replica films from GCs containing larger FAp crystals tend to crack upon detachment and consequently SEM micrographs had to be used. From those images, the determination of needle diameters is more difficult since the position of the visible cut through the needle can hardly be estimated. To ensure that the cut is not located in the periphery of the needle diameter, for longer ceramming times only those needles were included in the analysis which did contain inclusions formed upon crystallization of PSDs (these inclusions are known to rest in the middle of the needles, compare Figure 4b). The length was registered for those needles only that have facets running parallel to the sample surface or the width of which does not change along its length.

On the basis of the aforementioned rules, for a series of temperatures, the length of FAp needles was determined from between 100 and 200 needles each. The resulting length probability distributions are given in Figure 5. Except for 2 min, the length distributions are broad and asymmetric. This finding is not unexpected since already after casting a considerable number of crystallized PSDs are formed. Those crystals already start to develop the needle shape upon heat treatment while in parallel in some still existing PSDs, nucleation processes result in spherical apatite crystals, the needle-like growth of which is retarded in time.

Although much more effort had to be made for the glass ceramics heat-treated for 2 h, only those FAp needles were counted, the length *and* diameter of which were clearly detectable. The resulting diameter versus length plot is shown in Figure 6. Form this diagram, a linear average dependence between needle width and length can be deduced. Moreover, another important fact is proved by this plot. The FAp molar fraction determined by ^{31}P MAS NMR (Figure 3) is approximately constant. If, under such conditions, the average FAp needle diameter and length are steadily increasing, coarsening of FAp (compare average FAp needle volumes given in Table 1) requires the dissolution of smaller FAp needles, resulting in a decreased number density of FAp crystals. From Figure 6 it is evident that needle growth and dissolution follow the same time dependence (otherwise, instead of the linear dependence shown in Figure 6 two branches of data points would occur). During a very extensive inspection of the sample heat-treated for 2 h, no FAp needle lengths smaller than 1500 nm were detected. This might be explained as follows. It is known from the theory of particle coarsen-

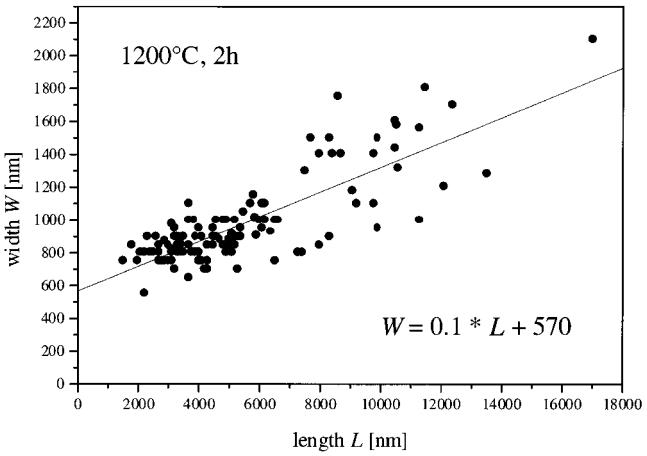

Figure 6. Distribution of simultaneously registered length and diameter of FAp needles heat-treated at 1200 °C for 2 h. The straight line represents the linear regression according to the equation given in the plot.

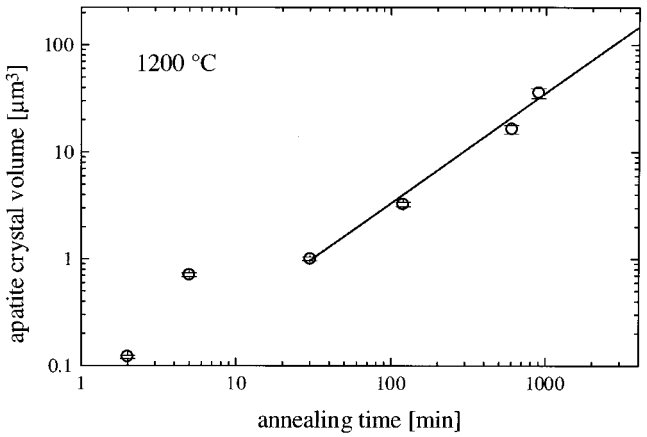

Figure 7. Annealing time dependence of the mean FAp needle volume (double-logarithmic plot). Upon heat treatment at 1200 °C for more than 30 min, a linear dependence applies, which is represented by the linear regression line.

ing (see for example ref 4) that, with decreasing radius, r, of a precipitate, the dissolution rapidly increases according to

$$\frac{dr}{dt} \propto \frac{1}{kT}\frac{1}{r^2}\left[\frac{r}{\bar{r}} - 1\right] \quad (1)$$

with the critical radius $\bar{r}$ and the temperature T. Thus, it can be concluded that, in the steady state where the equilibrium concentration of the ambient glass is adjusted, apatite crystals of <1.5 μm size are very susceptible to dissolution. Moreover, since the growth rate dr/dt is proportional to $1/T$, small apatite crystals still present at 1200 °C might be further subjected to dissolution upon cooling (strictly speaking, the critical radius $\bar{r}$ is dependent on T also) and consequently smaller needles are not observed.

According, for example, to ref 5 particle coarsening in the sense of Ostwald ripening is characterized by a typical kinetic behavior including the following:

(i) The mean particle volume is proportional to the time of heat treatment, t.

(ii) The coarsening phase exhibits a constant molar fraction and the particle number is inversely proportional to t.

(iii) The reduced particle size distribution $P(r/\langle r\rangle)$, where $\langle r\rangle$ denotes the mean particle radius, is time-invariant.

The first criterion can be easily proved by plotting the apatite-crystal volume given in Table 1 versus time. As can be seen in Figure 7, in fact, a linear dependence exists in the present case (note that for the sake of clearness a double-logarithmic presentation was chosen). Referring back to Figure 3, it becomes clear that the second condition is satisfied also since ^{31}P MAS NMR data prove that, between 5 and 900 min, the apatite molar fraction remains constant. The proof of a time-invariant reduced FAp-needle-length distribution $P(L/\langle L\rangle)$ is difficult since a rigorous treatment would require a joint registration of needle width and length (as presented in Figure 6) for a series of annealing times. Because of the enormous effort, such analyses were not performed but the inspection of Figure 5 shows that for heat treatments longer than 5 min, the shape of the needle-length distribution does not change notably. At this point, it should be noted that the needle-shape distributions observed do reflect the *unextruded* microstructure developed upon heat treatment of the *nonoriented* sample (needles may grow parallel and rather close to each other and interlocking may occur). Thus, the microstructure of the apatite glass ceramics before extrusion is very likely to have a much stronger influence on the FAp needle habit than the selection rules used for analysis.

Finally, it can be concluded that the coarsening kinetics of FAp needles—after the adjustment of the equilibrium composition in the glass matrix—corresponds to Ostwald ripening. The deviation of the particles from the spherical shape does not impair the consideration since—although Ostwald ripening was originally described for pure-element, spherical precipitates—for example, Li and Oriani[6] modified the theory for cases of nonspherical and multielement precipitates.

At this point it is worth noting that, in another, even more complex glass-ceramics material in the SiO_2–Al_2O_3–Na_2O–K_2O–CaO–P_2O_5–F^- system with minor additions of CeO_2, Li_2O, ZrO_2, B_2O_3, and TiO_2, apatite needles were reported to coexist with isometric leucite crystals. Müller et al.[7] have investigated the time dependence of those apatite needles with very simple experimental means (nonoriented needles, image analysis of standard SEM micrographs). Although their data consequently do rest on a number of assumptions not required in the present study due to the availability of *grain-oriented* samples, essentially the same time dependence was found. A direct comparison of both studies is impaired by severe differences in the composition of the glass ceramics (Müller et al. reported an apatite molar fraction more than 1 order of magnitude below the values found in the present study, and the maximum apatite needle length found in the apatite-leucite glass ceramic is also 1 order of magnitude smaller). Nevertheless, the tendency to form crystalline needles seems to be an inherent property of apatite unless the development of the anisotropy is outweighed by a

(4) Verhoeven, J. D. *Fundamentals of Physical Metallurgy*; John Wiley & Sons: New York, 1975.

(5) Gutzow, I.; Schmelzer, J. *The Vitreous State*; Springer: Berlin, 1995.

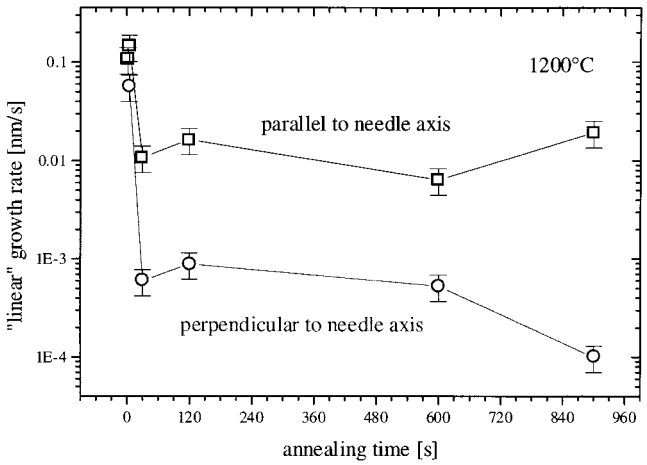

Figure 8. Quasi-linear growth rates (1200 °C) parallel and perpendicular to the FAp needle axis determined according to eqs 2 and 3 on the basis of time intervals.

deviation from enriched growth in the initial phase of crystallization.[1]

Returning to the average needle length and width values given in Table 1, the time dependence of growth rates parallel (v_z) and perpendicular (v_x) to the needle axis can be derived according to

$$v_x^{\text{time}} = \frac{W^{\text{sample1}} - W^{\text{sample2}}}{2 \cdot \Delta t^{\text{sample2-sample1}}} \tag{2}$$

$$v_z^{\text{time}} = \frac{L^{\text{sample1}} - L^{\text{sample2}}}{2 \cdot \Delta t^{\text{sample2-sample1}}} \tag{3}$$

The evaluation of all time intervals given in Table 1 results in the growth-rate values shown in Figure 8. Although error bars are of considerable size, two growth modi can be clearly discerned. Within the first 5 min, that is, under conditions of enhanced supersaturation (cf. ref 1 for the time dependence of the glass-matrix composition), the growth rates both along and perpendicular to the needle axis are on the order of several nm/s. Since v_z is more than 3 times larger than v_x, needlelike-shaped crystals are developed. After the equilibrium composition of the host glass is established, growth rates drop by 1 (parallel to the needle axis) to 2 (perpendicular to the needle axis) orders of magnitude. Consequently, the aspect ratio is increasing with time.

3.3. Thermodynamic Description of Apatite-Needle Growth. One possible reason for anisotropic growth rates due to kinetic effects is the combination of spiral growth along the needle axis (i.e., the crystallographic *c* axis of FAp) with normal growth perpendicular to it. In the following, it will be demonstrated that thermodynamic considerations are capable of explaining the occurrence of needlelike-shaped FAp crystals under such assumptions.

At steady state, the aspect ratio, *A*, is determined by

$$A = \frac{v_z}{v_x} \tag{4}$$

As needlelike crystals are observed, the width, *x*, of which is only about a micron, it shall be assumed that the mechanism of growth in the *x*-direction is controlled by two-dimensional nucleation, while in the *z*-direction it is controlled by a screw dislocation mechanism (spiral growth). The mechanisms of crystal growth are discussed in detail elsewhere (see refs 5 and 8) and in general the growth rate is given by

$$v \sim \Omega\left[1 - \exp\left(-\frac{\Delta\mu_{\text{cr}}}{RT}\right)\right] \tag{5}$$

where the parameter Ω accounts for the mechanism of growth, *R* is the gas constant, and *T* the temperature. The supersaturation of the elements contained in apatite, $\Delta\mu_{\text{cr}}$, is defined as

$$\Delta\mu_{\text{cr}} = RT \ln \frac{C}{C_{\text{cr}}} \tag{6}$$

with the concentration of the elements composing FAp in the melt, *C*, and the equilibrium concentration of FAp, C_{cr}.

For spiral growth

$$\Omega \sim \Delta\mu_{\text{cr}} \tag{7}$$

applies while in the case of a two-dimensional nucleation mechanism, Ω is determined by the rate of formation of two-dimensional nuclei, so that

$$\Omega \sim \exp\left(-\frac{B}{\Delta\mu_{\text{cr}}}\right) \tag{8}$$

In eq 8 *B* stands for

$$B = \frac{\pi\sigma^2 V N_{\text{a}} d_{\text{o}}}{RT} \tag{9}$$

with the specific free surface enthalpy σ, the molar volume *V*, Avogadro's number N_{a}, and the mean interatomic distance, d_{o}.

When eqs 7 and 8 are taken into account, the aspect ratio can be expressed in the form

$$A \sim \Delta\mu_{\text{cr}} \exp\left(\frac{B}{\Delta\mu_{\text{cr}}}\right) \tag{10}$$

The manner in which *A* is changing with temperature is seen from the derivative:

$$\frac{\partial A}{\partial T} \sim \left(1 - \frac{B}{\Delta\mu_{\text{cr}}}\right) \exp\left(-\frac{B}{\Delta\mu_{\text{cr}}}\right) \frac{\partial \Delta\mu_{\text{cr}}}{\partial T} \tag{11}$$

The term $\partial\Delta\mu_{\text{cr}}/\partial T$ can be estimated by considering that $\Delta\mu_{\text{cr}}$ can be written as

$$\Delta\mu_{\text{cr}} = \Delta\mu_{\text{liq}} + \frac{\Delta H_{\text{m}}}{T_{\text{m}}} \Delta T \tag{12}$$

with the supersaturation of the elements contained in PSDs, $\Delta\mu_{\text{liq}}$:

(6) Li, C. Y.; Oriani, R. A. In *Oxide Dispersion Strengthening*; Ansell, G. S., Cooper, T. D., Lenel, F. V., Eds.; Metallurgical Society Conference, Vol. 47; Gordon and Breach: New York, 1968; p 431.
(7) Müller, R.; Abu-Hilal, L. A.; Reinsch, S.; Höland, W. *J. Mater. Sci.* **1999**, *34*, 65.
(8) Gutzow, I.; Kashchiev, D.; Avramov, I. *J. Non-Cryst. Solids* **1985**, *73*, 477.

$$\Delta\mu_{liq} = RT \ln \frac{C}{C_{liq}} \quad (13)$$

(C_{liq}: concentration of the elements composing PSDs) resulting in

$$\frac{\partial \Delta\mu_{cr}}{\partial T} = \frac{\partial \Delta\mu_{liq}}{\partial T} - \frac{\Delta H_m}{T_m} \quad (14)$$

We know that most PSDs are growing at 800 °C ($\Delta\mu_{liq}$ *is positive)* and are dissolving at 1200 °C ($\Delta\mu_{liq}$ *has become negative*). This means $\Delta\mu_{liq}$ decreases with temperature, so that the right-hand side of eq 14 is always negative. Therefore, according to eq 11, the aspect ratio will increase with temperature as soon as

$$B > \Delta\mu_{cr} \quad (15)$$

It is easy to prove that this condition is always fulfilled if one relates the surface energy to the melting enthalpy (see refs 9 and 10) according to

$$\sigma = \alpha \frac{\Delta H_m}{V^{2/3} N_a^{1/3}} \quad (16)$$

where $\alpha \approx 0.5$. When eqs 6, 9, and 15 are taken into account, one finds that eq 14 leads to

$$\left(\frac{\Delta H_m}{RT}\right)^2 > \frac{C}{C_{cr}} \quad (17)$$

a condition that is always fulfilled.

It follows that under the assumption of either normal or spiral growth the shape will change from isometric at 800 °C to needlelike at 1200 °C.

3.4. Growth Shape versus Equilibrium Shape: The Effect of Long-Term Heat Treatment. In the present glass ceramics, the kinetics of growth results in a growth shape, which is very different from the equilibrium shape. After long-term annealing (80 h at 1200 °C), several 10 mm large, blocklike FAp crystals are formed at the expense of FAp needles (Figure 9). In contrast to the growth habit (determined by the growth rates ratio only), the equilibrium form (representing the morphology with minimum free energy for a given volume) is dependent on the surface energies along different crystallographic directions. Since the equilibrium form has nothing to do with the growth rates and there is no reason the growth form should approach the equilibrium form, there is no contradiction between the blocklike equilibrium form and the theoretical derivation, explaining the elongated growth.

The relaxation to the equilibrium form after long annealing times limits the aspect ratio of needlelike FAp crystals that can be obtained by thermal treatment at 1200 °C. The aspect ratio of 15:1 observed after 15 h of annealing at 1200 °C, however, is absolutely sufficient for the preparation of textured GCs with an extraordinary degree of grain orientation.[2]

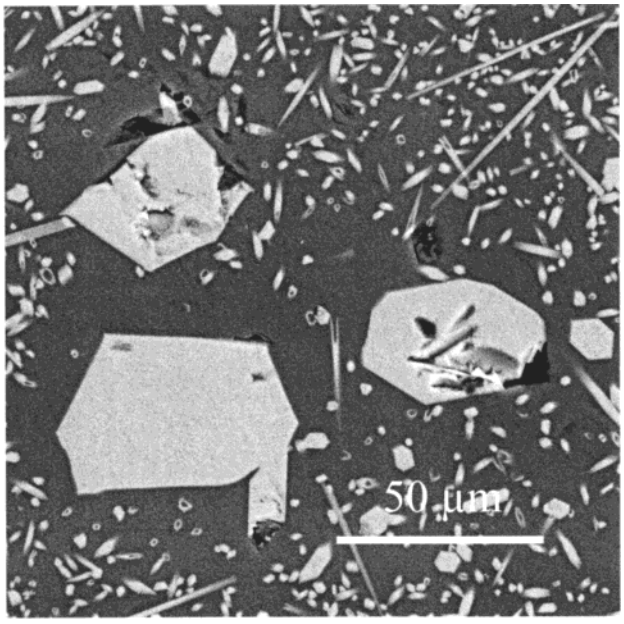

Figure 9. SEM micrograph of the glass ceramics after heat treatment for 80 h at 1200 °C.

4. Conclusion

On the basis of the joint analysis of TEM and SEM micrographs on the one side and TEM EDXS and ^{31}P MAS NMR experiments on the other side, the growth of fluorapatite needles in $SiO_2-Al_2O_3-CaO-P_2O_5-K_2O-F^-$ glasses upon heat treatment at 1200 °C is shown to follow the criteria for Ostwald ripening.

Between 30 min and 15 h of heat treatment at 1200 °C, the molar fraction of fluorapatite remains constant, within this time interval, the average apatite needle volume increases proportional to the annealing time, and the reduced needle-length distribution is invariant.

A theoretical treatment based on different growth modi along and perpendicular to the needle axis is capable of explaining the needle shape observed at 1200 °C and the absence of the needle habit upon thermal treatment of the same glass at 800 °C.

After 80 h of annealing at 1200 °C, fluorapatite needles start to dissolve since larger, blocklike apatite crystals representing the equilibrium form are formed. Consequently, there is an upper limit for the achievable fluorapatit aspect ratio, but for the synthesis of grain-oriented glass ceramics by extrusion a length-to-width ratio of 15:1 (15 h at 1200 °C) is highly sufficient.

Acknowledgment. This work was supported by the Deutsche Forschungsgemeinschaft, Bonn Bad Godesberg, Germany, within the Contract INK/6. We are indebted to Dr. G. Carl, Otto-Schott-Institut, FSU Jena, for stimulating discussions.

CM001204H

(9) Zanotto, E. *J. Non-Cryst. Solids* **1987**, *89*, 361.
(10) Avramov, I.; Keding, R.; Rüssel, C. *J. Non-Cryst. Solids* **2000**, *272*, 147.